Nano Express

INCLUSIVE PUBLISHING TRUSTED SCIENCE

PURPOSE-LED PUBLISHING™

PAPER • **OPEN ACCESS**

Enhancing water permeability in thin-film nanocomposite membranes utilizing electrospun recycled PET and graphene oxide

To cite this article: Mantsopa Koena Zamisa *et al* 2025 *Nano Ex.* **6** 015012

View the article online for updates and enhancements.

You may also like

- Effect of chain extenders on mechanical and thermal properties of recycled poly (ethylene terephthalate) and polycarbonate blends
Y Srithep, D Pholharn, A Dassakorn et al.
- Exploring the efficiency of green synthesized silver nanoparticles as photocatalysts for organic dye degradation: unveiling key insights
Aman Sharma, Sachin Sunny, James Arulraj et al.
- Fatigue life analysis and damage evaluation in glass fiber reinforced composite materials based on recycled polyethylene terephthalate
Ashwani Kumar Singh and Raman Bedi

This content was downloaded from IP address 146.64.81.209 on 03/03/2026 at 09:02

NANO EXPRESS

PAPER

Enhancing water permeability in thin-film nanocomposite membranes utilizing electrospun recycled PET and graphene oxide

Mantsopa Koena Zamisa[1,2], **Suprakas Sinha Ray**[2,3], **Makungu Marco Madirisha**[4,5], **Vincent Ojijo**[2], **Tumelo Seadira**[1], **Rotimi Emmanuel Sadiku**[6], **Neeraj Kumar**[2] and **Jonathan Orasugh**[2]

[1] Department of Chemical and Materials Engineering, College of Science, Engineering and Technology, University of South Africa, PO Box 1710, Johannesburg, South Africa
[2] Centre for Nanostructures and Advanced Materials, DSI-CSIR Nanotechnology Innovation Centre, Council for Scientific and Industrial Research, Pretoria 0001, South Africa
[3] Department of Chemical Sciences, University of Johannesburg, Doornfontein 2028, Johannesburg, South Africa
[4] Department of Civil Engineering, College of Science, Engineering and Technology, University of South Africa, PO Box 1710, Johannesburg, South Africa
[5] Chemistry Department, College of Natural and Applied Sciences, University of Dar es Salaam, PO Box 35061, Dar es Salaam, Tanzania
[6] Division of Polymer Technology, Department of Chemical, Metallurgical and Materials Engineering & Institute of Nanoengineering Research, Tshwane University of Technology, South Africa

E-mail: zamism@unisa.ac.za **and** mantsopazamisa@gmail.com

Keywords: graphene oxide, electrospun recycled polyethylene terephthalate, thin-film nanocomposite membranes, water permeability, sustainable materials

Supplementary material for this article is available online

OPEN ACCESS

RECEIVED
8 June 2024

REVISED
19 August 2024

ACCEPTED FOR PUBLICATION
14 November 2024

PUBLISHED
24 February 2025

Original content from this work may be used under the terms of the Creative Commons Attribution 4.0 licence.

Any further distribution of this work must maintain attribution to the author(s) and the title of the work, journal citation and DOI.

Abstract

Addressing the challenge of low permeability in Thin-Film Nanocomposite (TFNC) membranes is crucial for improving water filtration efficiency. Despite advancements in membrane technology, the interface between the substrate and active layer remains a critical research gap affecting overall permeability. This study aims to fill this gap using electrospun recycled polyethylene terephthalate (rPET) substrates combined with graphene oxide (GO). A vacuum-assisted self-assembly method was employed to coat microporous rPET substrates with GO. Extensive characterization techniques, including Scanning Electron Microscopy (SEM), Transmission Electron Microscopy (TEM), x-ray diffraction (XRD), Fourier Transform Infrared Spectroscopy (FTIR), and Brunauer–Emmett–Teller (BET) analyses, demonstrated the uniform GO layer formation on rPET substrates, indicating enhanced structural and operational efficiency. The integration of GO resulted in a crystalline structure modification, improved surface morphology, and increased water permeability. The optimized rPET-GO membranes showcased a significant decrease in water contact angle to approximately 93 degrees, denoting enhanced hydrophilicity and, consequently, better permeability compared to uncoated rPET membranes. Despite increased hydrophilicity, the membranes exhibited reduced but stable permeability rates, highlighting the effectiveness of the GO and rPET blend in advancing membrane functionality. These findings mark a significant advancement in membrane technology, offering enhanced water permeability efficiency and paving the way for a substantial impact on sustainable water management. Additionally, this study underscores the importance of recycling in developing advanced materials for environmental applications.

1. Introduction

To address the global challenges of water scarcity and pollution, advancements in membrane technology, particularly pressure-driven Thin-Film Nanocomposite (TFNC) membranes, have emerged as promising solutions for efficient water filtration and desalination [1]. These membranes use nonporous thin film active layers for ion rejection, while the underlying substrate offers mechanical support to the delicately thin active layer. These membranes continuously undergo performance improvements such as permeability enhancement

© 2025 The Author(s). Published by IOP Publishing Ltd

to reduce energy (pressure) requirements. Although much of this focus has been on refining the active layer [2, 3], the role of the substrates beneath is also crucial for the membranes' overall effectiveness. These substrates not only contribute to mechanical support but also significantly influence the membranes' filtration capabilities, impacting both flux and separation efficiency [4, 5].

The performance of Thin-Film Nanocomposite (TFNC) membranes is significantly influenced by the structure of the substrate layer, including its pore structure, sizes, and porosity. These characteristics directly impact the formation and efficacy of the active layer, which is crucial for the membrane's ability to separate and filter [6]. The substrate not only provides mechanical support but also plays a critical role in determining the membrane's overall permeability by minimizing the resistance to water flow through the support layer. In the process of interfacial polymerization (IP), which is key to forming the active layer, the substrate's properties influence crucial aspects such as the deposition and diffusion of monomers, and ultimately the active layer's thickness, density, and morphology [6–9]. This interplay between the substrate's structure and the active layer's formation underscores the substrate's importance in the development and performance of TFNC membranes, impacting both the efficiency of water filtration and the energy required for the process.

The use of highly porous microfiltration (MF) electrospun nanofibrous membrane (ENMs) as alternative support layers to the currently used phase inverted membranes can help improve separation performance in terms of improved membrane permeability and minimized water flow resistance [10, 11]. However, the large pore sizes, roughness, and hydrophobicity of ENMs are not ideal for forming thin-film active layers, resulting in defects and weak adhesion strength between the substrate and the thin-film active layer. Various polymers such as polyacrylonitrile (PAN) [12], polyimide [13], Polyvinylidene fluoride (PVDF) [14], polysulfone (PSF) [15], etc, have been electrospun as substrates for TFNC in various applications including (forward osmosis (FO), nanofiltration (NF), and pressure-retarded osmosis (PRO) systems [15, 16]. Recently, the use of PET ENMs [17, 18], and increase in interest in the use of recycled PET [19] in wastewater treatment [20], even in its recycled form, has opened new avenues in the fields of water purification (e.g. heavy metals removal), biomedical [21, 22] and food technologies (e.g. apple juice clarification) [21]. The rPET ENMs have been applied as good crude oil adsorbents in a study by Topuz *et al* In their unmodified form, the microporous and hydrophobic nature of the rPET, with water contact angle of 137 degrees, was highly beneficial in terms of oil sorption performance. The interaction between the hydrophobic benzene rings in the rPET structure and the non-polar hydrocarbons of the oil was through the intermolecular forces (i.e. van der Waals dispersion forces). With these forces of attraction, the good adsorption capacity of 14 g g^{-1} was therefore attained [23]. Zhao *et al* produced hydrophilic PET ENMs with a combination of micro- and nano-sized fibers with the help of additives, using melt electrospinning. The resulting PET ENMs with reduced pore sizes were able to reject titania nanoparticles (TiO_2 NPs) at 95% MF efficiency with the flux of 7900 $Lm^{-2}\,h^{-1}$ [24]. Maryam *et al* incorporated metal oxides (ZnO/ y-FeOOH NPs) into the rPET matrix for nanofiltration (NF) of heavy metals and obtained good water permeability and high rejection rates: pure water flux of 169.39 $kg.m^{-2}\,h^{-1}$ and ~95% lead rejection at 0.5 bar pressure. The incorporation of metal oxide NPs into the rPET polymer matrix led to the reduction in the resulting rPET ENMs surface roughness, increase in porosity and decrease in mean pore radius enhancing rejection capabilities (through charge effects, chelating mechanisms and size exclusions of the hydrated radii of the heavy metals [25]. On the other hand, as the microporous ENMs do not structurally meet the requirements of pressure-driven membrane processes (nanofiltration (NF) and reverse osmosis (RO)), particularly for rejection of smaller salt ions and therefore at higher pressures exceeding 1 bar. It is quite common to perform the necessary surface modifications to construct new denser membranes [26–29]. The surface modifications of ENMs include surface coatings by hydrophilic polymers or nanomaterials such as graphene oxide (GO) nanosheets [7, 30]. Thus, the thin layer coated onto the ENM can serve as an interlayer (between the ENM substrate and thin film active layer) to provide a smoother hydrophilic platform for depositing or coating the active layer. The coating of GO sheets as active or interlayers for NF has been performed on various ENMs substrates such as PAN, polyesters, and other polymers with aromatic π-systems, either by dip-coating or vacuum assisted filtration techniques [31, 32], while only a few studies have made use of PET, particularly the electrospun and recycled counterparts [33, 34].

Despite these advancements, a significant research gap remains, in optimizing the interface between the substrate and active layer to enhance overall membrane permeability. This study addresses this gap by introducing a unique approach in membrane technology using graphene oxide (GO) nanosheets and electrospun recycled polyethylene terephthalate (rPET) to enhance the permeability of TFNC membranes for NF and RO processes. GO nanosheets, employed as laminar layers, function as an interlayer between the substrate and the active layer, revolutionizing the traditional structure of pressure-driven membranes. The process involves coating electrospun microporous rPET substrates with a composite of GO using a vacuum-assisted self-assembly (VASA) filtration method. This method is noted for its simplicity and effectiveness, allowing precise assembly of intercalated GO interlayers. By addressing the limitations of traditional substrates and active layers, this approach offers a significant leap forward in creating effective membranes with enhanced

permeability. Consequently, this advancement holds considerable potential for mitigating global water scarcity and pollution, marking a crucial step towards sustainable water management and environmental preservation. Moreover, the utilization of recycled materials like PET emphasizes the importance of recycling in developing advanced materials for environmental applications, promoting sustainability and reducing waste.

2. Materials and methods

2.1. Materials

Recycled PET (rPET) pellets were obtained from Mpact Recycling, South Africa. The viscosity average molecular weight of the rPET polymer solution was 73.06 kg mol^{-1}. Hydrochloric acid (HCl), sulphuric acid (H_2SO_4), potassium permanganate ($KMnO_4$), hydrogen peroxide (H_2O_2), and graphite (powder, <20 μm, synthetic), were all purchased from Merck, South Africa. All chemicals used in the experiments were of research grade and used as received. The density of the synthesized GO powder was 1.86 g cm^{-3} as measured by a pycnometer (Micromeritics AccuPyc II 1340, USA).

2.2. Preparation of nanomaterials

2.2.1. Synthesis of GO

Graphene Oxide (GO) sheets were synthesized by utilizing a modified version of Hummers' method, as outlined in the work of Kumar *et al* [35]. The method makes use of H_2SO_4 and $KMnO_4$ whereby $NaNO_3$ and H_3PO_4 were excluded to avoid the release of toxic gases. The method makes use of a low-cost scalable route for high-grade GO production while using minimum chemical reagents and reducing the synthesis time. The typical procedure was as follows: concentrated H_2SO_4 was added to 40 g of graphite powder and stirred for 60 min at 25 °C. The small portions of 160 g of $KMnO_4$ (~5 g) were added slowly to the above mixture under stirring, for 17 min (1 graphite: 91.5 H_2SO_4:4 $KMnO_4$). The exothermic reaction mixture reached a maximum temperature of 52 °C, after which, started to decrease, and the reaction temperature was then set to 50 °C in a reactor. This continued for 6 h under stirring to allow the reaction to complete. The reaction mixture turned brownish to indictate complete oxidation process. Following the completion, the reaction mixture was cooled naturally, then poured on ~4 L of ice water with 1% of H_2O_2 solution. To remove M_n impurities and acid residues, the solution was further washed with deionized water and centrifuged several times at 4000 rpm. The collected residue was again mixed with 5% HCℓ to remove the remaining salts and centrifuged (4000 rpm) using deionized water (1 L) and the supernatant was discarded away. The dark-brownish product (graphite oxide) obtained was re-dispersed in deionized water and ultrasonicated for 90 min to get GO sheets. Finally, the centrifuged product was dried in a vacuum oven at 60 °C to obtain a dried GO sample after 24 h.

The process is illustrated in figure 1.

2.3. Preparation of rPET as the substrate

The preparation of ENMs substrate (electrospun rPET) using electrospinning technique, was performed as stated in our previous work [36].

2.3.1. Modification of rPET substrate by deposition of the GO

Composite membranes of electrospun rPET-GO were fabricated by depositing the GO onto the electrospun rPET substrate. GO was first produced in various concentrations utilizing diverse solvents, detailed in subsection 2.3.1.1. This modification process employed a vacuum-filtration process known as vacuum-assisted self-assembly (VASA) technique, which is illustrated in figure 2.

2.3.1.1. Effect of the solvent system on the preparation of GO

GO dispersions were prepared by adding 10 mg of GO powder into 10 ml of different solvents, to achieve a concentration of 1 mg ml^{-1}. These solvents were acetone (Ace), deionized water (H_2O), isopropyl alcohol (IPA), and ethanol (EtOH). The GO dispersions were sonicated to form a uniform dispersion and then deposited onto the rPET substrates using the VASA technique. After coating, the obtained rPET-GO membranes were oven-dried at 90 °C for 5 min. The resultant membranes, were labeled according to the solvent used; i.e. rPET-GO-Ace, rPET-GO-EtOH, rPET-GO-IPA, and rPET-GO-H_2O for acetone, ethanol, IPA and H_2O, respectively, and served to evaluate how different solvents affect the adherence of GO to the rPET surface. It was discovered that water was the superior solvent for GO application, prompting its exclusive use in subsequent experiments investigating the influence of GO concentration variations on the substrate's properties.

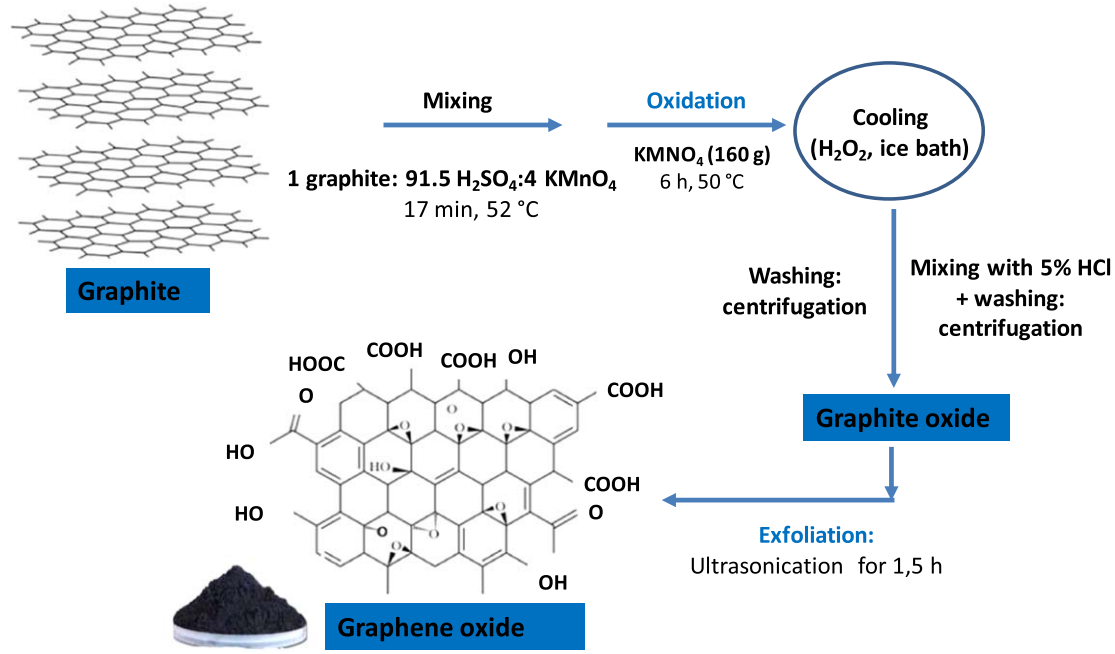

Figure 1. Synthesis of GO using improved Hummers method. Reproduced from [35], with permission from Springer Nature.

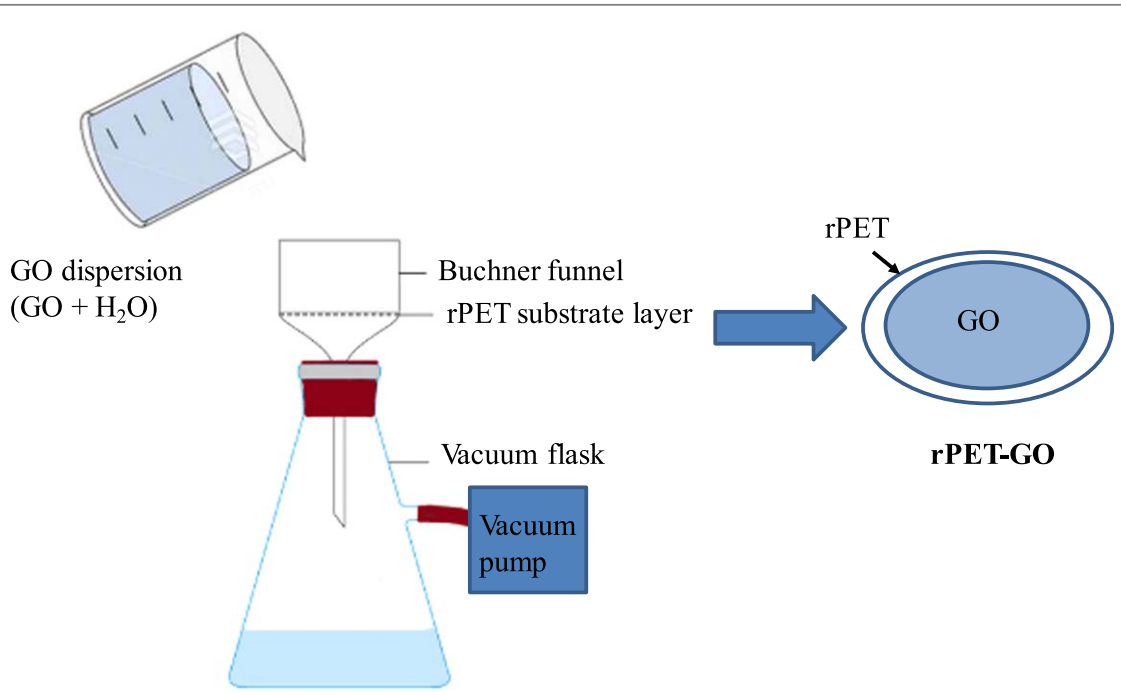

Figure 2. Preparation of GO-coated rPET substrate (GO-rPET) by Vacuum-assisted self-assembly (VASA).

2.3.1.2. Effect of GO loading

The study investigated the effect of GO content on the d-spacing between the GO layers, by varying the amount of GO powder (i.e. quantities of 10 to 50 mg). These were added to 50 ml of deionized water to achieve concentrations from 0.2 to 1 mg ml^{-1}. After sonication for 10 min, a uniformly exfoliated GO suspension was obtained. These suspensions were designated as GO-10, GO-15, GO-25, and GO-50, to represent the amount of GO they contained. The sonicated dispersions were then applied to the rPET substrates using a vacuum-assisted filtration method. The resulting membranes labelled as rPET-GO-10, rPET-GO-15, rPET-GO-25, and rPET-GO-50, respectively. Membranes with 10 and 15 mg of GO resulted in a uniform coating, , and were therefore selected for further studies.

Table 1. Parameters for permeability test of membranes.

Membrane	Volume of collected water (ml) at different time			Membrane cross section areas		
	1 min	10 min	30 min	A1 $\times 10^{-4}$ (m^2)	A2 $\times 10^{-3}$ (m^2)	A3 $\times 10^{-3}$ (m^2)
rPET	0.125	0.35	0.75	1.77	1.08	5.027
rPET-GO-10	0.016	0.06	0.045	1.77	1.08	5.027
rPET-GO-15	0.01	0.055	0.032	1.77	1.08	5.027

2.4. Characterization of rPET, GO and rPET-GO

The surface morphology of rPET, GO, and rPET-GO membranes was investigated using the scanning electron microscopy (SEM) (JEOL JSM-7500F, Tokyo, Japan), operating at an accelerating voltage of 3 kV and an emission current of 10 μA under high vacuum (9.5×10^{-5} Torr). Prior to SEM imaging, the membrane samples were mounted onto aluminium stubs using double-sided tape and then coated with carbon to prevent charging and ensure good conductivity under the electron beam. Additionally, the surface features of rPET, GO, and the rPET-GO composite membranes were examined using Multimode Atomic Force Microscopy (AFM, NanoScope Version (R) IV, London, UK), which also measured the height, lateral dimensions, and the thickness of the GO sheets. For AFM analysis, GO suspensions were spread onto silicon wafer substrates, left to air dry, and then placed on an AFM stage for assessment.

Chemical functionalities within the rPET, GO, and rPET-GO membranes were analyzed through Attenuated Total Reflectance Fourier Transform Infrared (ATR-FTIR) Spectroscopy using a Perkin-Elmer Spectrum 100 spectrometer, spanning a wavelength range from 800 to 4000 cm^{-1} with 32 scans at a resolution of 4 cm^{-1}. Furthermore, x-ray diffraction (XRD) analysis, utilizing a PANanalytical X'Pert PRO instrument (Netherlands) and equipped with nickel filtered CuKα radiation ($\lambda = 1.5406$ Å), was conducted to assess the chemical and crystalline composition. It was specifically used to identify crystalline phases and to calculate the interlayer spacing between nanosheets using the Bragg equation, as depicted in equation (1) [37]:

$$2d.\ \sin\theta = n.\lambda \tag{1}$$

Where d is the interlayer spacing of GO nanosheets (nm) within the GO coating (rPET-GO), θ is the diffraction angle, $n = 1$ is the order of reflection, and $\lambda = 1.540598$ and is the wavelength of x-ray.

Hydrophilicity was assessed using a DSA100 contact angle analyzer from KRUSS, Germany, through water contact angle (WCA) measurements at ambient temperature, to evaluate the surface wettability of the rPET/GO mats. This was achieved by employing the sessile drop technique, where the membrane samples were positioned on a stage, and droplets ranging from 6 to 8 microliters (μL) of deionized water were precisely applied to the surface with a micro-syringe. A real-time camera recorded the droplet's profile, to calculate the WCA.

The specific surface area of GO was determined using the N_2 adsorption–desorption isotherms using the Micromeritics (TriStar II 3020 Version 3.02) instrument, by applying the Brunauer–Emmett–Teller (BET) technique. Prior to analysis, the samples were degassed under high temperature of 150 °C, for 4 h, in order to remove any gaseous impurities within the powdered samples. Additionally, the thermal stabilities of rPET and GO were analyzed through Thermogravimetric Analysis (TGA) using a PerkinElmer TGA 4000, at a consistent heating rate of 10 °C min^{-1} in an air atmosphere, a temperature range of 25 to 800 °C.

The high-resolution transmission electron microscopy instrument (HRTEM; JEOL, 2100F-JEM,Japan) operated at 200 kV, was used to investigate the morphology and structural features of the synthesized GO.

2.5. Membrane permeability performance

The water permeance of the membranes was measured on a homemade dead-end vacuum filtration device with an effective area of 14.51 cm^2 under a pressure difference of 1.0 bar at room temperature. The parameters used during permeance tests are shown in table 1. The total volume of deionized water used as the feed to test the pure water permeance of rPET, rPET-GO-10, and rPET -GO-10 was 1000 ml. Therefore, we directly recorded the permeance of rPET, rPET-GO-10, and rPET -GO-15 membranes when the feed pressure reached 1.0 bar until the target duration of 30 min was reached. The permeance (J) (L m^{-2} h^{-1} bar^{-1}) was calculated according to equation (2).

$$J = \frac{V}{A\Delta tP} \tag{2}$$

where V (L) is the volume of permeated water, A (m^2) is the effective membrane area, Δt (h) is the permeate time, P (1.0 bar) is the pressure difference, respectively.

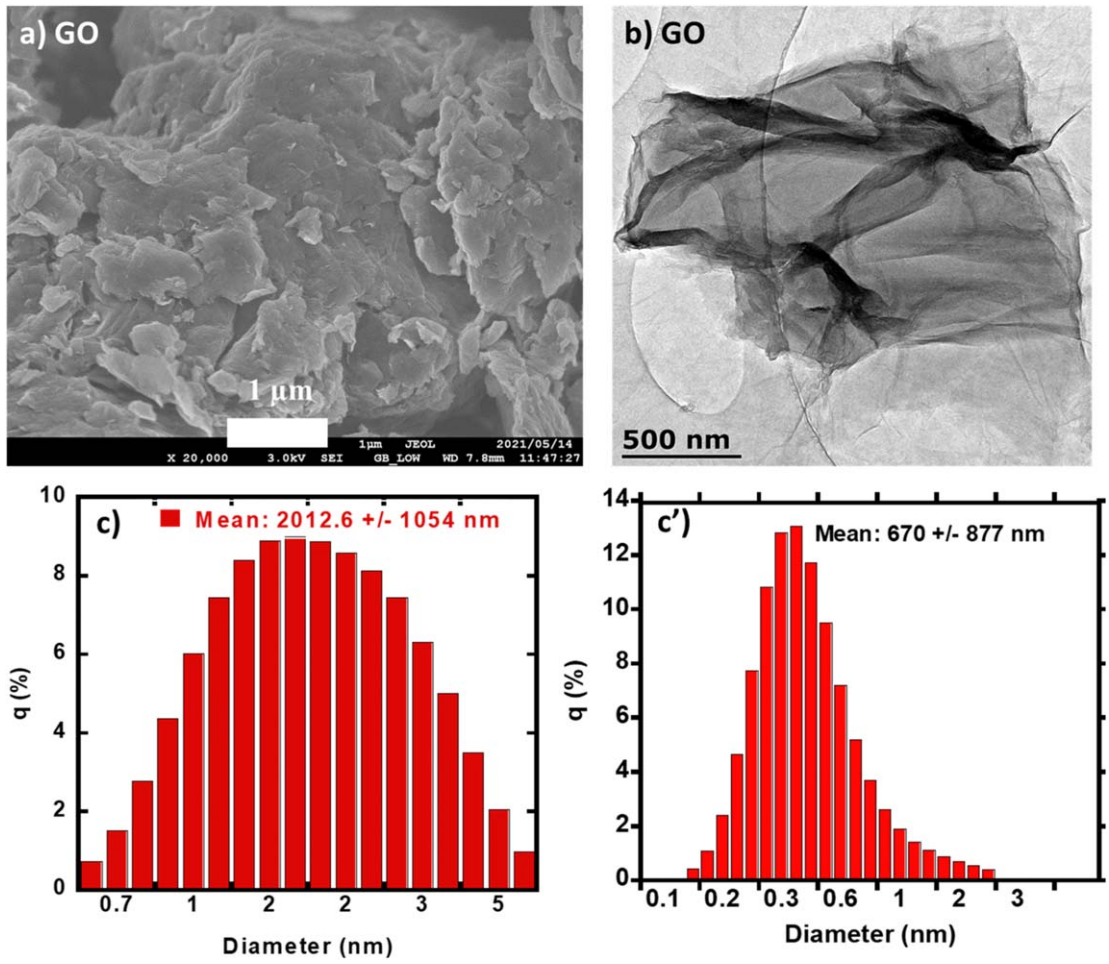

Figure 3. (a) SEM and (b) TEM images depicting the surface morphologies of GO powder. (c) Particle size distribution of GO before sonication, (c') Particle size distribution of GO after sonication.

3. Results and discussions

3.1. Morphology of the synthesized GO

The morphological characteristics of the synthesized GO are presented with SEM and TEM images as depicted in figures 3(a) and (b), respectively. The SEM image from figure 3(a) shows multilayers of re-stacked exfoliated GO sheets. The sheets also display a crimped appearance with some folds and corrugations at the edges as observed on the TEM image in figure 3(b). The GO sheets have lateral dimensions of a few hundred nanometres, as also observed in other studies [35].

The nanoscale morphologies before sonication display the GO powders in their aggregated form. The sizes of the GO sheets ranged from 700 nm to 5 μm, with an average of 2 μm as indicated in figure 3(c), measured by dynamic light scattering (DLS). Following sonication, the GO exhibit reduced aggregation, with particle sizes now spanning from 100 nm to 2.5 μm and a mean size of 670 nm as shown in figure 3(c′). This sonication process aimed to disperse the GO clusters into less aggregated sheets. The dispersed GO sheets were expected to stack as a uniform nanosheet multilayer, forming a smooth coating (or interlayer) on the rPET substrate (section 3.2.2).

Moreover, the AFM images in figure 4 corroborated the SEM and TEM observations. Specifically, figure 4(a), which illustrated the height profile for agglomerates, indicated that the GO sheets, prior to sonication, formed agglomerates due to their inherent tendency to stack, resulting in structures of varied heights and indicating a level of pre-exfoliation aggregation. The calculated average dimensions of the agglomerated GO sheets (before sonication) were established as 15.5 nm in thickness and dimensions of 0.246 × 1.872 μm in width and length, respectively, detailed in figures 4(b) and (b'). The identified thickness of 15.5 nm implies an assembly of approximately 15 GO sheet layers. Conversely, post-sonication measurements revealed a diminished thickness of 2.9 nm, indicative of the presence of single sheets or a minimal stack of 2 to 3 GO sheet layers, as depicted in figures 4(c), (c'), (d), and (d').

In figure 5, the BET curves for the GO powder exhibit characteristics of a mesoporous texture, aligning with Type IV isotherms typically indicative of such structures. The GO's surface area was determined to be 15 $m^2 g^{-1}$,

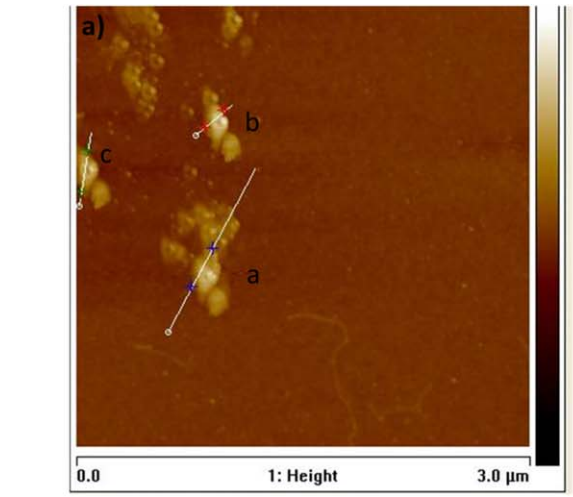

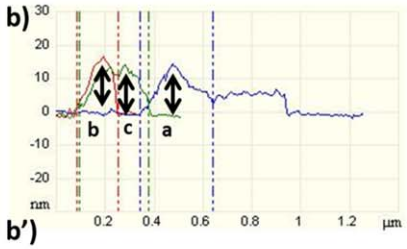

b')

Particle	Thickness	Width (µm)	Length (µm)
a	15.1	0.298	3.089
b	17.6	0.161	1.91
c	13.7	0.279	0.617
Average	15.46	0.246	1.87

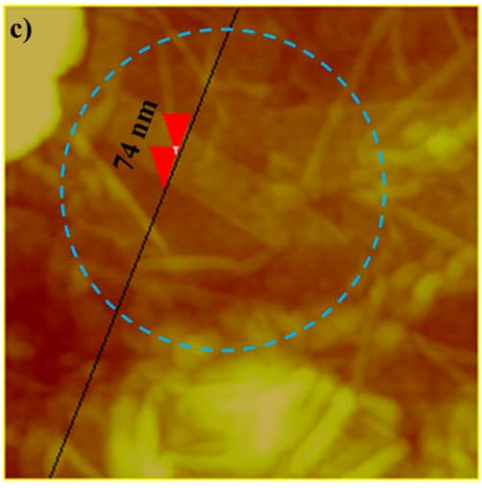

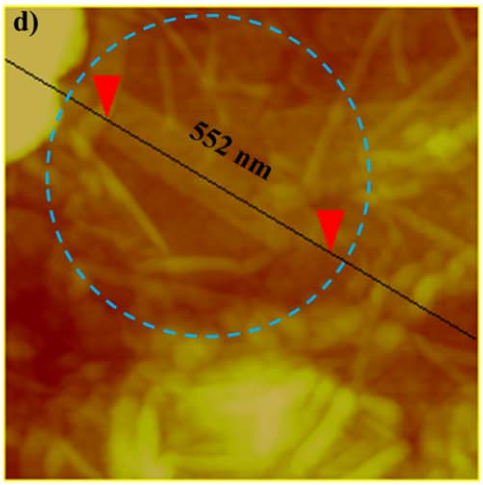

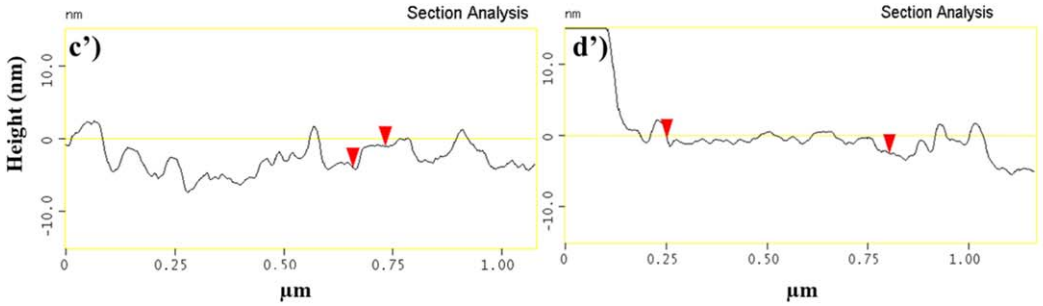

Figure 4. AFM micrographs of GO before and after sonication: (a) height profile for agglomerates labeled a, b, and c, before sonication, (b) and (b') lateral sizes: length, thickness, and width before sonication, (c), (c') and (d), (d') width, and length and thickness of the GO single or monolayer sheets after sonication.

which is significantly lower than the values often cited in the literature, typically greater than 70 $m^2 g^{-1}$ [38, 39]. This discrepancy can likely be ascribed to the agglomeration of the GO particles, which underscores the necessity of sonication prior to application to disperse these aggregates and potentially expose more surface area.

The desorption limb of the isotherm further reinforces the complexity of the GO's pore architecture, suggesting a heterogenous assortment of mesopores interspersed with larger voids. Such a distinctive porosity profile is instrumental in defining the adsorptive behavior of GO. These surface and structural characteristics are crucial for GO's efficacy in various functional roles, including its use in sensor technologies, filtration systems, and as a supportive matrix for catalytic processes. The lower surface area observed may impact these applications, as it suggests a reduced number of active sites for interaction with other substances. Therefore, optimizing the sonication process could be key to enhancing the performance of GO in its intended applications. Acknowledging the importance of maximizing the available surface area for these applications, we employed sonication intending to disperse the agglomerates and enhance the surface area of the GO.

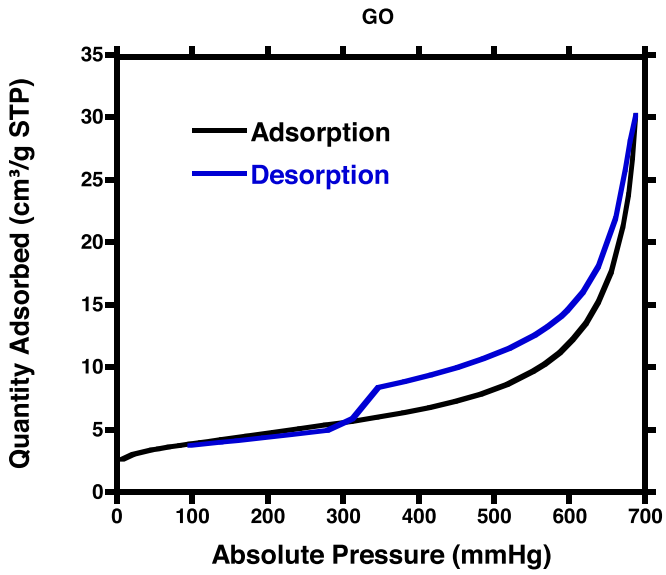

Figure 5. Nitrogen adsorption–desorption of GO powder.

3.2. Modification of rPET membrane surface: coating of rPET substrate by GO-interlayer

3.2.1. Effect of solvent system

Vacuum-assisted self-assembly (VASA) is a simple membrane fabrication technique performed by a vacuum filtration process using nanoparticle dispersions such as nanosheets/rods to produce highly ordered uniform films. It is a flow-directed filtration of GO nanosheet dispersions either in an aqueous or organic media. In this technique, the GO dispersions containing disordered nanosheets will eventually generate a thin film layer of highly ordered GO-layered membrane [35]. In this section, the previously electrospun hydrophobic rPET substrate was modified by deposition or coating of GO layer as a hydrophilic interlayer. The GO dispersions were prepared using various solvents (H_2O, IPA, ethanol, and acetone, to form GO-H_2O, GO-IPA, GO-EtOH, and GO-Acetone dispersions, respectively). These were used to evaluate the effectiveness of GO coating or deposition on the rPET. The coated membranes are shown in figure 6. The coating using GO-H_2O and GO-EtOH dispersions was not coated as a film, instead, they were deposited as agglomerates onto the rPET fibers. The poor deposition was due to the microporous structure of the rPET fibrous membrane. The dispersed GO particles were too small to be captured by the large pores of the electrospun rPET membrane. In addition, the GO sheets agglomerated and formed larger clusters, which were then captured between the fibers and loosely bound onto the rPET surface. When coated onto membranes, the thin GO laminar sheets tend to fold and wrinkle, thus resulting in aggregates. The GO-acetone coating, on the other hand, was uniform, as visually observed in figure 6(c'). However, the even coating showed that microscopically, some cracks were visible, as observed in the SEM image in figure 6(c). Acetone is known as a good solvent for GO coating because of its higher evaporation rate. The GO-IPA coating, on the other hand, was evenly coated and showed the desired morphology of a film layer, but not uniform throughout the membrane surface. The sheets were uniformly stacked as ordered layers instead of agglomerates. However, the incorporation of GO into the polymer matrix of rPET fibers during electrospinning did not have much effect in improving the hydrophilicity of the membrane, as previously stated in our previous work [36], as most of the GO was embedded within the fibers. However, the effect of GO was more pronounced when the sheets were coated onto the membrane surface rather than embedding them within the polymer matrix of the fibers.

The XRD plots in figure 7 show that both rPET and GO peaks are present in all GO-coated rPET membranes, except the rPET-GO-H_2O membrane. GO dispersed in H_2O was poorly deposited on the substrate due to the agglomerates rather than a film layer formation, as observed in figures 6(b) and (b') above. Therefore, the GO peak was not evident for the rPET GO-H_2O sample. The GO peak at 2 theta of 10.25° showed a slight shift to a higher angle (11.04–11.25°) in all the other GO solvent systems, with additional peaks appearing on the rPET-GO-acetone membrane. The *d*-spacing was only reduced from 0.86 of GO powder to 0.79 nm for rPET-GO-ipa and 0.4 nm for rPET-GO-EtOH and rPET-GO-acetone. The use of various solvents resulted in a decrease in the d-spacing and hence the decrease in the GO nanochannel size within the GO sheets. Other factors that affect the GO coating are the coating time, volume, and concentration of the GO solution (GO loading) [40].

Dispersing the GO in various solvents had little effect on the rPET structure, except for the rPET-GO-Ace sample. Acetone is known to promote crystallinity in the amorphous rPET substrate as it does on most polymers

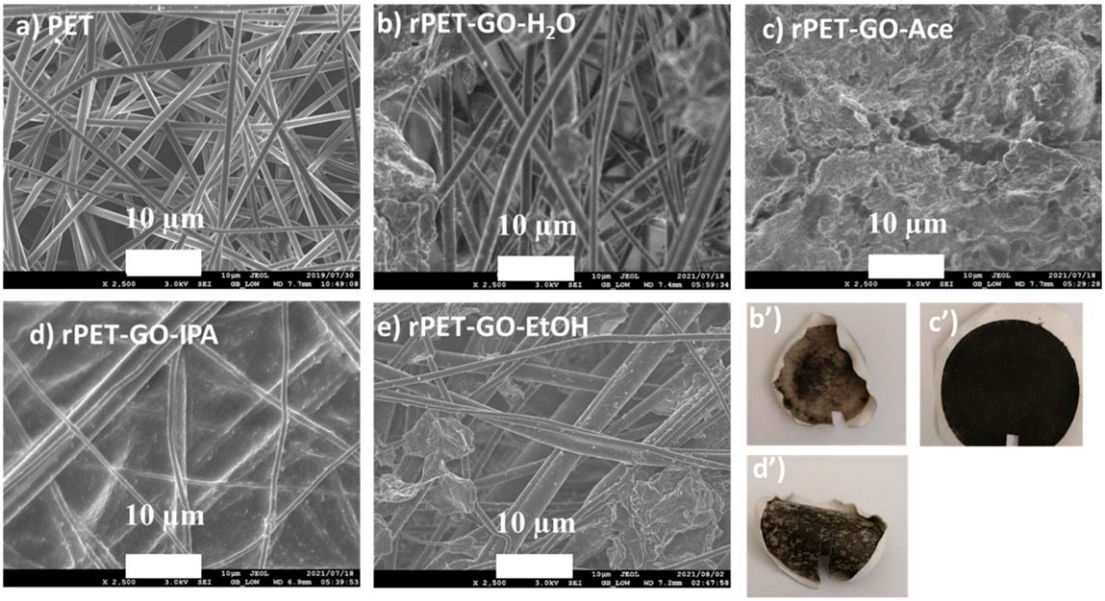

Figure 6. SEM images depicting a) rPET substrate before coating with GO dispersions prepared using various solvents namely, (b) water (H_2O), (c) acetone (Ace), (d) isopropanol (IPA), and (e) ethanol (EtOH); Photographic images of the GO-coated rPET substrates (b')–(d').

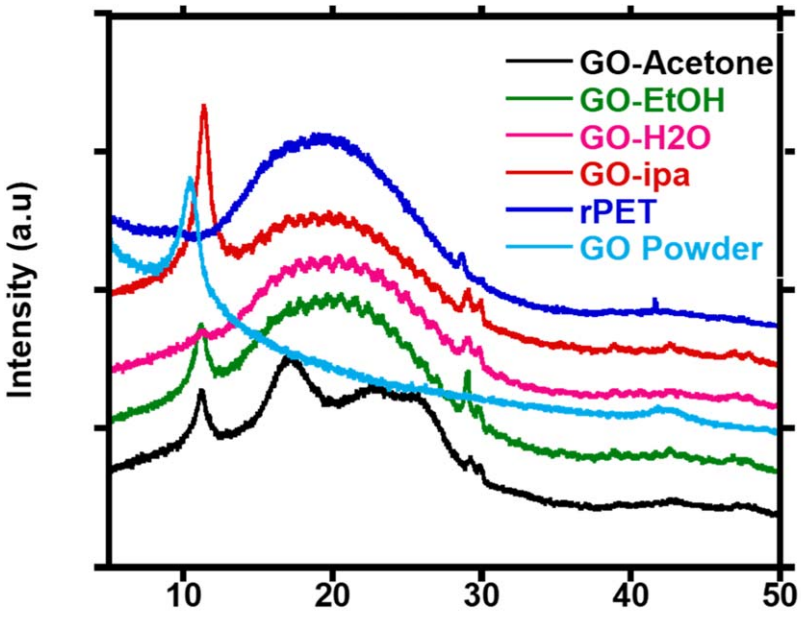

sample	2θ	d-spacing (nm)
GO powder	10.25	0.86
rPET-GO-Ace	11.125	0.40
rPET-GO-EtOH	11.00	0.40
rPET-GO-ipa	11.375	0.79
rPET-GO-H_2O	n.a	

Figure 7. XRD patterns of rPET coated with GO dispersions prepared using various solvents.

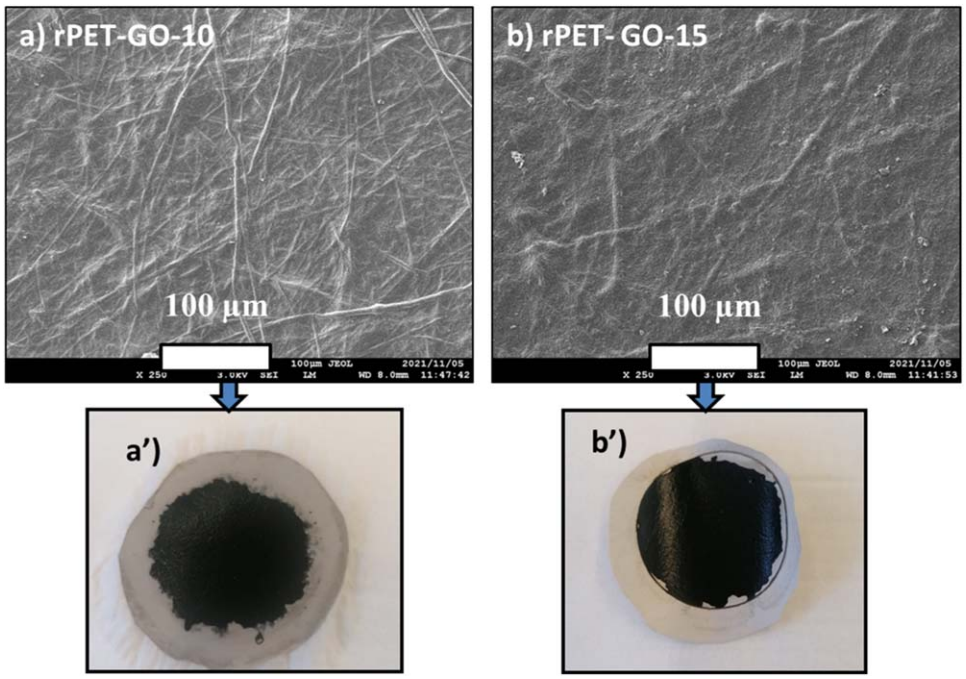

Figure 8. SEM images showing morphology of the GO coated rPET substrates at varying concentrations: (a) 10 mg GO (rPET-GO-10), (b) 15 mg GO (rPET-GO-15). Digital photographs for coated rPET: (a') GO −10, (b') GO-15.

[40, 41]. This, however, due to membrane shrinkage, may adversely affect the rPET nanofibrous membrane structure, e.g. reduction in the porosity. According to the coating quality of the GO onto the rPET membranes using the various solvents, the rPET-GO-ipa did form a smooth GO film coating layer, however, in a discontinuous manner. Therefore, coating using H_2O as a solvent will be investigated further. In the next section of solvents used, H_2O was the selected solvent used to investigate the effect of solvent volume on the GO coating. The volume of GO-H_2O dispersion was then increased from 10 ml to 50 ml. Of the volumes used (10, 25, and 50 ml), the 50 ml volume successfully coated the rPET substrate and formed a smooth homogeneous film layer, as shown in the following section.

3.2.2. The effect of GO loading and coating of GO onto rPET substrate

GO at varying amounts of 5, 10, and 15 mg, was dispersed in 50 ml DI H_2O to study the effect of GO dosage on the coating and the *d*-spacing of the coated GO sheets. The SEM images in figures 8(a) and (b) show a smoother morphology of the GO-coated rPET membranes as compared to the previously prepared in figure 6. As observed in the SEM images in figures 8(a) and (b), the compact and densely packed GO thin films were uniformly coated and showed good affinity for the rPET substrate, unlike the loosely packed deposition of the GO sheets prepared using smaller volume of 10 ml solvents in figure 6. This was an indication that there may be a strong bond between the GO sheets and the substrate. The GO hydroxyl and carboxyl groups formed hydrogen covalent π bonds with the aromatic groups of the rPET substrate [42, 43]. The ordered stacking of the GO sheets was due to the sufficient liquid medium for the GO sheets to disperse (50 ml), whereas with the lower volumes of 10 ml, there was a high possibility for re-agglomeration of the dispersed GO sheets while colliding with one another, due to the confined space, when smaller volumes are used. Zhao and co-workers stated that the deposition of the GO sheets is a process that follows a possible mechanism where the dispersed GO sheets are immobilized on the rPET substrate through hydrostatic forces (i.e. force caused by the pressure loading of GO dispersion acting on the underlying rPET substrate) during water or solvent removal (drying). This forms the first assembled layer of single GO sheets. As more GO comes into contact with the first assembled layer of GO sheets, hydrostatic force, and the solvent-mediated inter-sheet attractions, cause a new additional layer of GO sheets to form. The layering process repeats, and the film grows until all the GO dispersion is used up [44].

The fundamental issue for GO membranes is the control of the interlayer spacing to make it an effective ion separation membrane layer by enhancing its ion sieving effect [45]. The increased volume allows easier stacking of the GO sheets during vacuum filtration, thus forming an even, intact film without agglomeration [46].

Lower GO concentrations ($<$10 mg) appeared to be inadequate for the effective deposition on the rPET fiber substrate surface, whereas higher concentrations $>$ 15 mg seemed to be more susceptible to agglomeration. Therefore, GO contents of 10 and 15 mg were sufficient to form a uniform coating layer (figures 8(a), (b)).

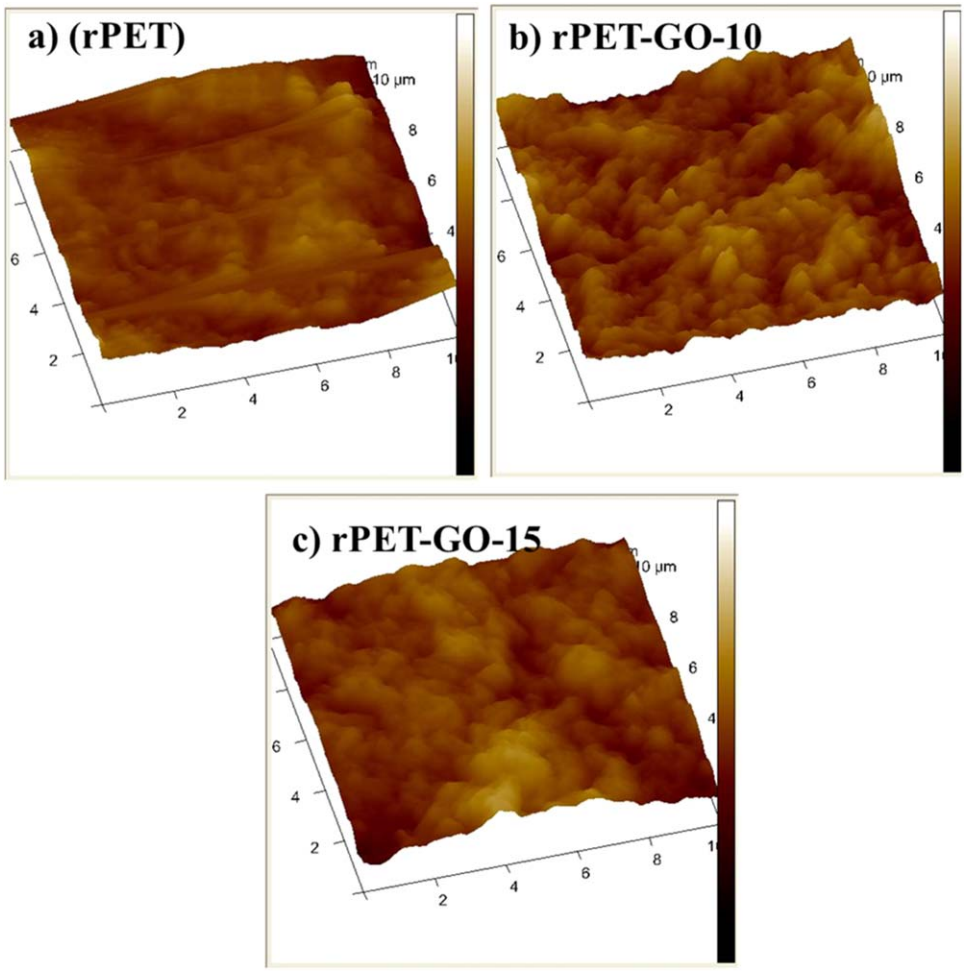

Figure 9. AFM micrographs of the electrospun rPET substrates: (a) rPET before coating, (b) rPET with GO surface coating at 10 mg GO content (rPET-GO-10), (c) rPET with GO surface coating at 15 mg GO content (rPET-GO-15).

Table 2. Surface roughness parameters of rPET before and after surface coating with GO.

Membrane	Rq (nm)	Ra (nm)	R_{max} (nm)
(rPET)	317	194	3022
rPET-GO-10	60.4	48	440
rPET -GO-15	80.8	63.1	603

Abbreviations: Rq = root mean square average of height deviations; Ra = average roughness; R_{max} = the maximum distance between the highest point and the lowest point on the 3D image profiles.

3.2.3. Surface features of the rPET-GO membranes

The three-dimensional AFM images of the membrane surfaces for electrospun rPET and rPET-GO (i.e. rPET substrate before coating and rPET coated with GO) are shown in figure 9. The brightness or colour variation depicts the height of the membrane surface. Brighter regions represent ridges, hence, a rougher surface. The roughness parameters, i.e. Ra and Rq, were captured at a scan area of 10 × 10 or 5 × 5 μm and are shown in table 2. Ra values are usually used to represent the surface roughness of membranes. The Ra for the pristine rPET was slightly reduced after the incorporation of GO within the fibers during electrospinning. For the GO-coated membranes (rPET-GO-10 and rPET-GO-15), the surface roughness was significantly reduced, from 194 nm for the rPET substrate before GO coating to 38 nm for GO-10. The improved surface smoothness, which increases with a decrease in GO content, from 48 nm for the rPET-GO-10 membrane (10 mg GO content) to 63.1 nm for the rPET-GO-15 membrane (containing 15 mg GO). However, based on the Cassie-Wenzel theory, these

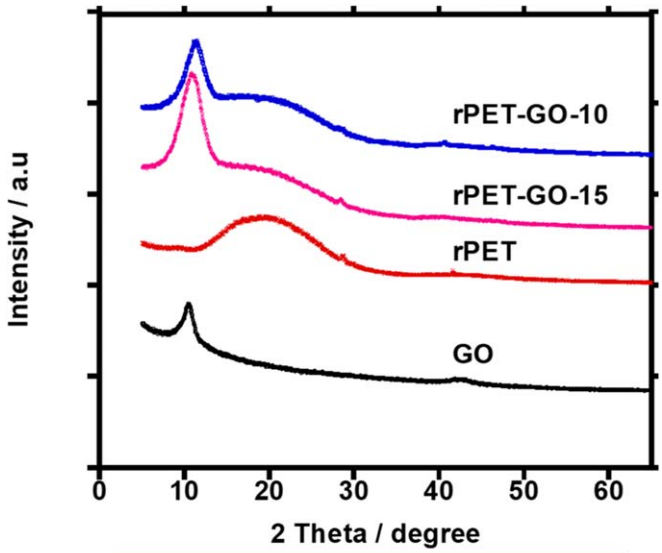

Sample	2 theta	d-spacing (nm)
GO powder	10.25	0.86
GO-rPET-10	11.13	0.80
GO-rPET-15	10.77	0.82

Figure 10. XRD patterns of GO powder, rPET, GO-coated substrates (rPET-GO-10 and rPET-GO-15).

findings contradict those in the study by Mehranbod, Khorram [47], who obtained an increase in surface roughness upon coating of ENMs substrate with GO, and emphasized that surface roughness translates to reduced WCA (hydrophilicity).

XRD was used to determine the phase, crystallinity, and *d*-spacing of the synthesized GO powders and the spacing between adjacent GO sheet layers in the laminated structure of the coated GO onto the rPET substrate (figure 10). For GO powder, a single sharp peak around 2θ value of 10.25° is equal to a *d*-spacing of 0.86 nm (8.62 Å) according to the Bragg equation (1), typical of GO laminate membranes. This also shows that the GO was well synthesized, as no additional graphite oxide peaks were evident. This means all the graphite oxide sheets were converted to graphene oxide (GO) during exfoliation. The small peak at 2θ of 42.06° shows that not all the graphite oxide was converted to GO (graphene oxide) during oxidation [46]. The interlayer spacing and nanochannel size of GO membranes (as GO-coated substrates) can be regulated by the intercalation of particles between the GO nanosheets.

In figure 11, the GO peak (2θ of 10.25°) is visible for the membranes coated with GO, with the peak intensity increasing with GO amount, i.e. highest for the rPET-GO-15 membrane. A slight shift to 10.77 ° and 11.13° for rPET-GO-15 and rPET-GO-10, respectively, shows that there is a slight decrease in *d*-spacing with a decrease in GO amount. The decrease was from 0.86 nm for bulk GO powder, to 0.82 and 0.79 for rPET-GO-15 and rPET-GO-10, respectively. This shows a tighter packing of the stacked GO sheets coated onto the membranes, as compared to the bulk GO powder. The broad amorphous rPET hump is observed at about 2θ (10°–30°).

The GO-coated membranes show the broad rPET hump to indicate that the GO coating does not disrupt the rPET substrates structure (rPET crystallinity was not disrupted by the physical interaction with GO as no new peaks emerged).

Figure 11 presents the FTIR spectra for graphene oxide (GO), recycled polyethylene terephthalate (rPET), and the GO-coated. The spectrum of GO is marked by distinct absorption bands linked to its oxygenated functional groups. A wide absorption band near 3400 cm^{-1} is indicative of O-H stretching vibrations from hydroxyl groups. Pronounced peaks near 1720 cm^{-1} are representative of the C=O stretching from carboxylic groups. Additional notable peaks around 1220 cm^{-1} correspond to epoxy groups' C–O stretching. Furthermore, the absorption bands in the vicinity of 1050 cm^{-1} correlate with the C–O stretching vibrations of the alkoxy groups.

For rPET, the FTIR spectra showed characteristics of ester absorptions with C=O stretching vibrations near 1710 cm^{-1} and C–O stretching vibrations in the region of 1100 to 1300 cm^{-1}. Additionally, the aromatic stretching of C=C stretching was typically observed around 1500–1600 cm^{-1}. The composite materials

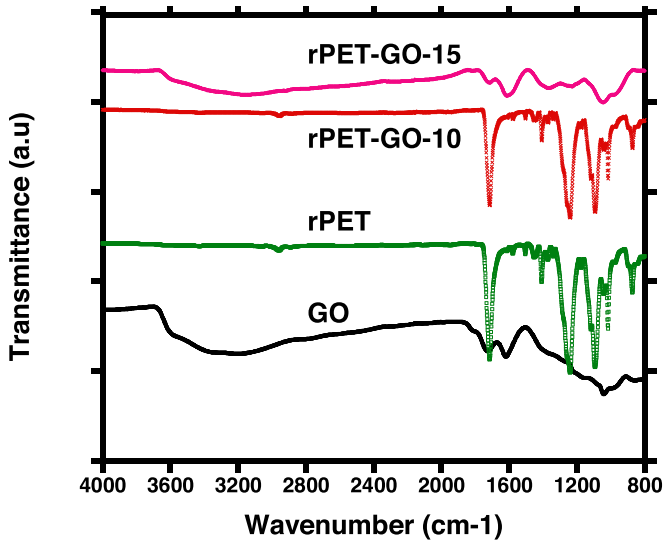

Figure 11. FTIR spectra of rPET substrates coated with GO (i.e. rPET-GO-10 and rPET-GO-15).

Table 3. Hydrophilicity of membranes.

Membranes	WCA (°)
(rPET)	120
rPET-GO-EtOH	139.10 ± 10
rPET-GO-Acetone	101.11 ± 11
rPET-GO-ipa	53.61 ± 6
rPET-GO-H_2O	21.13 ± 5
rPET-GO-15	93.38 ± 7
rPET-GO-10	93 ± 10

displayed a combination of the absorption features of GO and rPET. The loading of GO was observed to affect the intensity of the absorption bands corresponding to GO's functional groups. For instance, an increase in the concentration of GO (from rPET-GO-10 to rPET-GO-15) was observed to result in a more pronounced peak due to C=O stretching revealing a more interaction and well-coated on the rPET.

The FTIR results were consistent with the XRD results, which also confirmed an even and more uniform coating for rPET -GO-15, as compared to the rPET-GO-10. These results are also consistent with the SEM findings.

3.3. Performance evaluation of fabricated membranes

3.3.1. Hydrophilicity of membranes

Table 3 shows various membranes and their corresponding water contact angle (WCA) values, which serve as an indicator of hydrophilicity,the affinity of a material for water. Recycled polyethylene terephthalate (rPET) serves as the reference material and displays a moderate level of hydrophilicity with a WCA of 120 degrees. When rPET is combined with graphene oxide (GO) and ethanol, there is a marginal decrease in water attraction, as indicated by a higher WCA of 139.10 ± 10 degrees. In contrast, an acetone treatment enhances the membrane's affinity for water, reducing the WCA to 101.11 ± 11 degrees. The hydrophilicity markedly intensifies for rPET-GO treated with isopropanol, shown by a lower WCA of 53.61 ± 6 degrees, and it is even more pronounced when water is used in the treatment, lowering the WCA to a significant 21.13 ± 5 degrees. Nevertheless, these lower WCAs are attributed to clumping that leads to a non-uniform coating on the rPET surface. Furthermore, the quantities of solvents such as water and isopropanol were not fine-tuned to disperse the GO sheets properly, causing a chaotic deposition on the surface. However, for coatings in rPET-GO-15 and rPET-GO-10, with optimized solvent volumes and GO amounts, the WCAs are recorded at 93.38 ± 7 degrees and 93 ± 10 degrees, respectively, suggesting greater hydrophilicity than that of the untreated rPET.

In membrane technology, the affinity of a membrane for water, or hydrophilicity, typically has a direct impact on its permeability: the greater the hydrophilicity, the easier it is for water molecules to pass through.

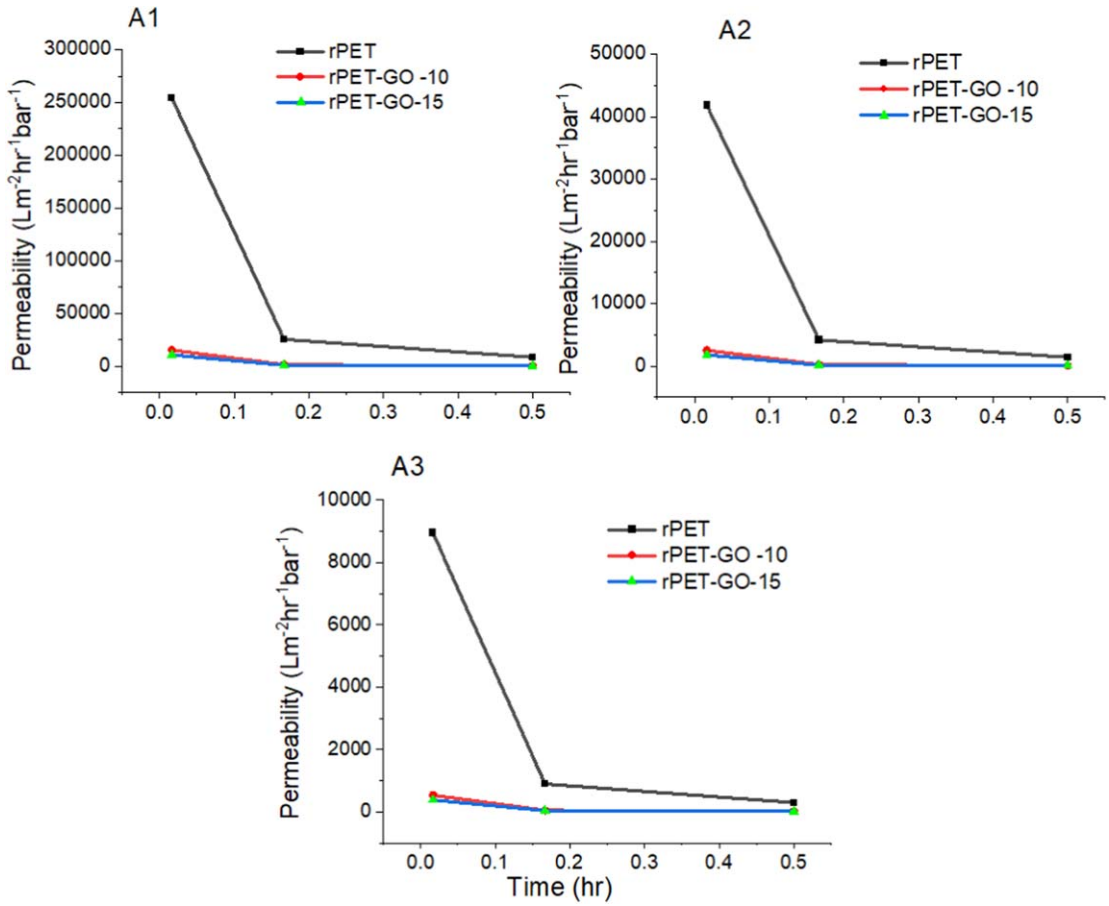

Figure 12. Comparative permeability of rPET, rPET-GO-10, and rPET-GO-15, considering their respective cross-sectional areas, (A1)–(A3).

This is because a hydrophilic surface creates a favourable environment for water interactions, facilitating its movement. The strategic modifications made to rPET with graphene oxide (GO) and a variety of solvents aimed at enhancing the membrane's surface properties, particularly to increase the rate of water passage for improved water filtration. The efficacy of these modifications in terms of permeability can be better understood through permeability tests. Such testing measures the capacity of water to penetrate the membrane, shedding light on the effects of the modified surface chemistry and texture on the membrane's performance in facilitating water flow.

3.3.2. Permeability of membrane

Figure 12 and Supplementary table 1 illustrate the permeability findings for rPET, rPET-GO-10, and rPET-GO-15, considering their respective cross-sectional areas. In figure 12(A1) (A1 implies cross-section area $= 1.77 \times 10^{-4}$), the initial high permeability observed for the unmodified rPET (owing to the highly porous or microporous nature that offers low resistance to water transport), which rapidly decreases, may still suggest rapid membrane wetting, followed by the establishment of a steady flow state through the pores of the membrane. The notable difference between the initial and subsequent permeability rates could be due to the immediate saturation of the smaller cross-sectional area of A1. The GO-modified membranes, rPET-GO-10 and rPET-GO-15, display a consistently lower permeability from the outset. This lower and stable flow rate across the smallest cross-sectional area, A1, suggests that the modifications lead to a more uniform and controlled flow, potentially due to the effect of GO layers on the membrane structure and pore characteristics. GO sheets deposited onto membranes offer mass transfer resistance which increases with an increase in GO loading or thickness [10].

For figure 12(A2) (A2 implies cross-section area $= 1.08 \times 10^{-3}$), the rPET membrane also shows a precipitous drop in permeability after the initial measurement. The larger cross-sectional area of A2 compared to A1 allows for a greater volume of flow initially; however, the decline suggests that the wetting effect reaches a limit quickly before stabilizing. As in A1, the rPET-GO-10 and rPET-GO-15 membranes maintain a low and stable permeability, which might be more desirable for applications that prioritise consistent performance over higher flow rate.

For figure 12(A3) (A3 implies cross-section area $= 5.027 \times 10^{-3}$) presents the lowest initial permeability among the three, which is logical given that A3 has the largest cross-sectional area. This inverse relationship between the cross-sectional area and the initial permeability might seem counterintuitive, but could be due to a more even distribution of the flow across the larger area, resulting in lower localised velocities. Again, the permeability for the modified membranes is consistently low, demonstrating a potential design feature of the GO modification that prioritizes stability and perhaps selectivity over volume throughput.

The high permeation of water through the microporous rPET membrane, despite the high water contact angle (hydrophobicity), is mainly attributed to the large pore size [48]. For the nanoporous GO sheets, on the other hand, water is transported through the distance between two adjacent GO nanosheets, which serve as a 2D nanochannel between the hydrophobic carbon walls, whereby the water permeates through the slip flow theory. This starts with the flow of water towards the space between adjacent sheets or defects where it collects, and then slips through the hydrophobic 2D channels [10]. Therefore, at the nanofiltration level, these hydrophilic GO membranes can offer ultrafast water transport for high flux performance [10]. Therefore, these findings signify the role of rPET in enhancing water flux in membrane-based water applications using TFNC membranes, as well as the role of the GO modification towards both the selectivity and flux enhancement of such membranes.

In summary, the unmodified rPET substrate experienced a significant decrease in permeability after filtration onset across all tested cross-sectional areas, indicating that factors other than compaction are at play, such as membrane wetting and the establishment of a flow equilibrium,since the pressure used was only 1 bar, ruling out compaction issues. The GO-modified membranes show much lower but consistent permeability rates across all cross-sectional areas, likely reflecting the impact of the GO layers on the flow dynamics and membrane pore structure. The uniform performance of the modified membranes regardless of cross-sectional area is significant, pointing to their potential in filtration applications where predictable and reliable performance (i.e., high membrane flux while maintaining selectivity toward contaminants) is critical. Their lower permeability suggests a trade-off between stability and high flow rates. Understanding this trade-off is vital for selecting the appropriate membrane type for specific filtration needs. Further studies, possibly including long-term filtration tests and analysis of the impact of GO on the membrane's microstructure, would provide deeper insights into optimising these materials for real-world applications.

Figure 13 and Supplementary table 2 show a comparative permeability of the rPET, rPET-GO-10, and rPET-GO-15 membranes over time at 1 bar pressure. Initially, at 0.0167 h, the rPET membrane allows for an exceptionally high volume of water to pass through, indicating an absence of initial resistance and possibly pointing to a phase where the pores are fully open and not yet affected by any filtering process. This is in contrast with the rPET-GO-10 and the rPET-GO-15 membranes, which displayed a much lower permeability right from the beginning. This suggests that the graphene oxide (GO) modifications alter the surface or pore characteristics, possibly creating smaller or fewer pores, leading to a reduction in flow rate compared to the unmodified rPET. Modification of rPET by coating with nanomaterials such as GO therefore, shows the potential growing interest in applying microporous ENs in applications that require membranes capable of removing the minutest of contaminants such as divalent and monovalent ions (e.g. desalination using TFNC membranes) [12, 49, 50].

Moving to the 0.167 h mark, there is a significant decrease in the permeability of the rPET membrane, levelling out to a rate more consistent with that of the GO-modified membranes. This sharp reduction could be indicative of the initial burst of flow reaching an equilibrium, or it could imply that the immediate high flow was due to transient conditions such as air being expelled from the membrane pores or the membrane being fully wetted. On the contrary, the permeability of rPET-GO-10 and rPET-GO-15 remains relatively unchanged, showcasing a consistent performance. The stability of these membranes could be a result of the GO providing a uniform flow path or offering resistance to fouling, which can be particularly advantageous for applications requiring controlled and reliable filtration processes.

By the time we observed the results at 0.5 h, the permeability rates for all membrane types were stabilized. The permeability of the unmodified rPET no longer showed the drastic fluctuations seen earlier , which could indicate that the initial rapid flow was not representative of its consistent performance. Conversely, the rPET-GO-10 and rPET-GO-15 maintained their initial low permeability levels, reinforcing the notion that the graphene oxide modification contributed to a steady and predictable membrane behaviour over time. The comparative analysis between the rPET-GO-10 and rPET-GO-15 membranes revealed minimal differences in permeability (mainly due to their hydrophilicity as also revealed by similar water contact angle values in table 3), suggesting that within the range of concentrations or treatments of GO between these two membranes, there was no significant impact on the water flow rate. This consistency is important for industrial and environmental applications where predictable outcomes are necessary.

In summary, these permeability profiles shed light on the short-term dynamics of the membranes under study, emphasizing the substantial influence of graphene oxide modification on the flow characteristics of rPET membranes. The data underscore the potential of GO-modified membranes to provide stable and reliable

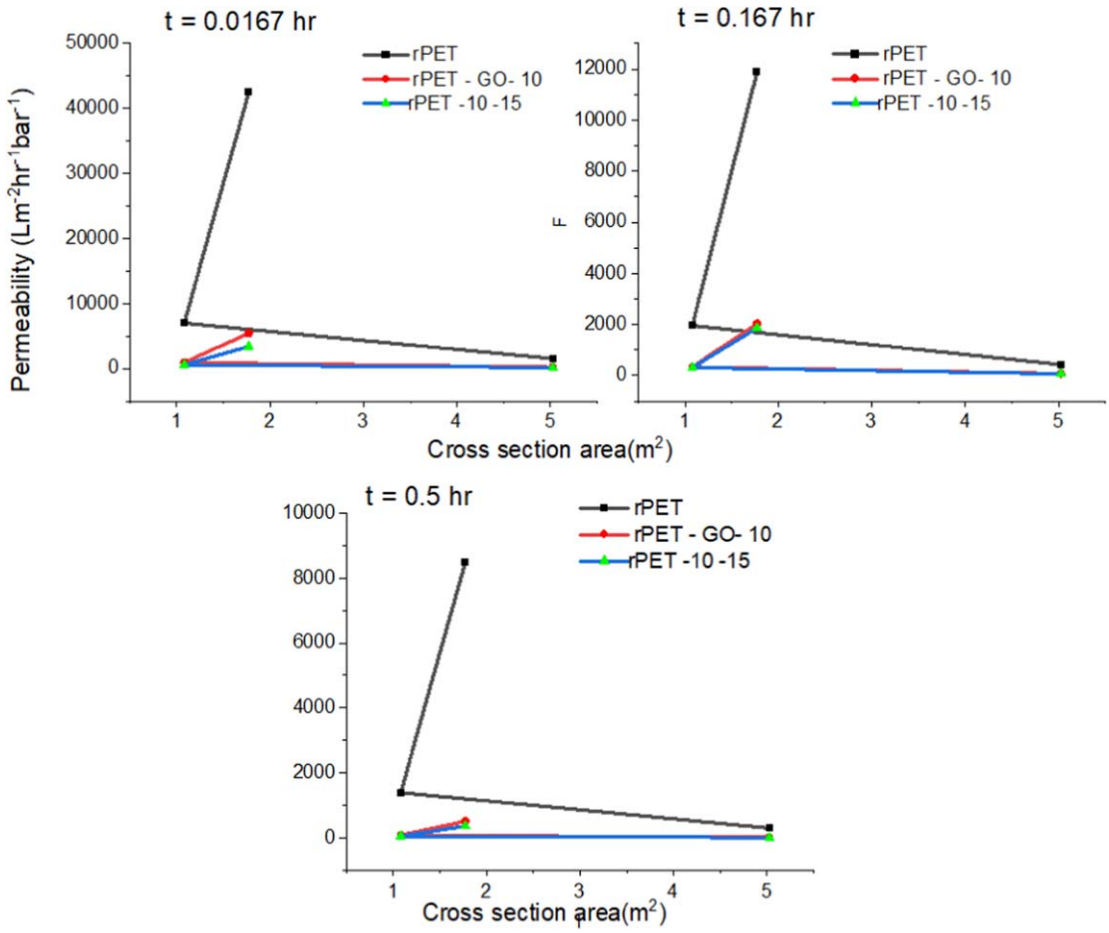

Figure 13. Comparative permeability of rPET, rPET-GO-10, and rPET-GO-15 membranes over time at 1 bar pressure.

performance, which is particularly beneficial for filtration applications where consistent quality is critical. For a more comprehensive understanding of the membranes' performance, particularly over prolonged durations and in varied operational conditions, further testing would be crucial.

4. Conclusion

This study addresses the critical issue of membrane permeability in Thin-Film Nanocomposite (TFNC) membranes by integrating electrospun recycled polyethylene terephthalate (rPET) substrates with graphene oxide (GO). Key findings reveal that the incorporation of GO enhances the structural and operational efficiency of the membranes, significantly improving water permeability. Characterization techniques such as SEM, TEM, XRD, FTIR, and BET confirmed the uniform formation of GO layers on rPET substrates, leading to crystalline structure modification and better surface morphology. The results have broad implications for the field of membrane technology, particularly in water filtration and desalination. By optimising the interface between the substrate and the active layer, this approach contributes to a deeper understanding and development of more efficient TFNC membranes. This advancement not only addresses the need for higher permeability but also supports sustainable water management practices by using recycled materials. Future research should focus on further optimising the composition of GO and rPET to enhance scalability and evaluate the long-term performance of these membranes in various filtration applications. Additionally, investigating the interaction between the membrane and different contaminants can provide insights into improving the selectivity and durability of TFNC membranes. This study acknowledges several limitations, including the potential variability in GO layer formation and the need for more extensive long-term performance testing. These factors may influence the interpretation of results and highlight the necessity for continuous refinement in membrane fabrication processes. In conclusion, this research marks a significant step forward in membrane technology, offering enhanced water permeability and paving the way for substantial advances in sustainable water management. The innovative blend of GO and rPET substrates demonstrates a promising solution to global

water scarcity and pollution, encouraging further exploration and application of these materials in real-world scenarios. Importantly, the use of recycled materials like rPET underscores the critical role of recycling in developing advanced, environmentally friendly materials, aligning with global sustainability goals and reducing waste.

Data availability statement

Data can be shared upon request. The data that support the findings of this study are available upon reasonable request from the authors.

Funding statement and acknowledgments

The authors acknowledge the Department of Science and Innovation (HGERA8X) the Council for Scientific and Industrial Research, CSIR (HGER74P), and the University of Johannesburg (86310) for the financial support. Furthermore, thanks are extended to CSIR, Tshwane University of Technology for providing laboratory space and academic assistance. Special appreciation is also given to Ms. Sharon Eggers and Dr Thomas Malwela for their support with Atomic Force Microscopy.

Conflict of interest

The author declares no conflict of interest.

ORCID iDs

Mantsopa Koena Zamisa https://orcid.org/0009-0006-1972-9303
Suprakas Sinha Ray https://orcid.org/0000-0002-0007-2595
Makungu Marco Madirisha https://orcid.org/0000-0002-4037-3974
Vincent Ojijo https://orcid.org/0000-0002-3473-6580
Tumelo Seadira https://orcid.org/0000-0001-6228-4393
Rotimi Emmanuel Sadiku https://orcid.org/0000-0002-8504-1041
Neeraj Kumar https://orcid.org/0000-0001-5019-6329
Jonathan Orasugh https://orcid.org/0000-0002-3680-3441

References

[1] Qasim M *et al* 2019 Reverse osmosis desalination: a state-of-the-art review *Desalination* **459** 59–104
[2] Khoo Y S *et al* 2022 Eco-friendly surface modification approach to develop thin film nanocomposite membrane with improved desalination and antifouling properties *J. Adv. Res.* **36** 39–49
[3] Ng Z C *et al* 2021 Thin film nanocomposite RO membranes: review on fabrication techniques and impacts of nanofiller characteristics on membrane properties *Chem. Eng. Res. Des.* **165** 81–105
[4] Ng Z C *et al* 2021 Improving properties of thin film nanocomposite membrane through polyethyleneimine intermediate layer: a parametric study *Sep. Purif. Technol.* **274** 119035
[5] Behdarvand F *et al* 2021 Polyvinyl alcohol/polyethersulfone thin-film nanocomposite membranes with carbon nanomaterials incorporated in substrate for water treatment *J. Environ. Chem. Eng.* **9** 104650
[6] Zabihi Z and Homayoonfal M 2021 Strategies to modify the structure of thin-film composite membranes for advanced separation of metronidazole antibiotic from wastewater *Polym. Adv. Technol.* **32** 4765–86
[7] Zhu X *et al* 2020 Ultrathin thin-film composite polyamide membranes constructed on hydrophilic poly(vinyl alcohol) decorated support toward enhanced nanofiltration performance *Environmental Science & Technology* **54** 6365–74
[8] Dlamini D S *et al* 2021 Fine-tuning the architecture of loose nanofiltration membrane for improved water flux, dye rejection and dye/salt selective separation *J. Membr. Sci.* **621** 118930
[9] Wu W *et al* 2021 Electrospun nanofiber based forward osmosis membrane using graphene oxide as substrate modifier for enhanced water flux and rejection performance *Desalination* **518** 115283
[10] Liu Z *et al* 2021 A facile and scalable method of fabrication of large-area ultrathin graphene oxide nanofiltration membrane *ACS Nano* **15** 15294–305
[11] Kim S, Heath D E and Kentish S E 2020 Composite membranes with nanofibrous cross-hatched supports for reverse osmosis desalination *ACS Appl. Mater. Interfaces* **12** 44720–30
[12] Al-Furaiji M *et al* 2020 Preparation of thin-film composite membranes supported with electrospun nanofibers for desalination by forward osmosis *Drink. Water Eng. Sci.* **13** 51–7
[13] You X *et al* 2021 Electrospun polyimide-based thin-film composite membranes for organic solvent nanofiltration *J. Membr. Sci.* **640** 119825
[14] Qanati O *et al* 2023 Thin film composite on sulfonated PVDF electrospun and its performance in nanofiltration *Korean J. Chem. Eng.* **40** 1141–50

[15] Hadipour A et al 2024 Benzenesulfonamide-functionalized electrospun polysulfone as an antibacterial support layer of thin-film composite pressure-retarded osmosis membrane: fabrication and performance evaluation International Journal of Environmental Research 18 37
[16] Ji K et al 2023 Research progress of water treatment technology based on nanofiber membranes Polymers 15 741
[17] Xiong Q et al 2024 A smart superwetting PET-anthocyanin membrane for pH monitoring in water and emulsion separation J. Ind. Eng. Chem. 132 507–17
[18] Agboola O et al 2023 Statistical analyses of pore radii on the performance of PET-nanocomposite membranes in the removal of iron and anions from Ibeshe River S. Afr. J. Chem. Eng. 44 89–102
[19] Hussain N et al 2021 Synthesis of highly conductive electrospun recycled polyethylene terephthalate nanofibers using the electroless deposition method Nanomaterials 11 531
[20] Ali B T I et al 2023 Utilization of polyethylene terephthalate (PET) plastic bottle waste as membrane with several modifications for the removal of chromium ions in wastewater Mater. Today Proc. 74 433–7
[21] Nojavan C et al 2024 Potential use of electrospun poly(ethylene terephthalate)/carbon nanotubes containing aspirin in vascular tissue engineering application Fibers Polym. 25 71–81
[22] Sepehri R et al 2022 Heparin-coated poly(ethylene terephthalate)/graphene oxide nanofibers used for vascular tissue engineering application Fibers Polym. 23 3012–21
[23] Topuz F, Oldal D G and Szekely G 2022 Valorization of polyethylene terephthalate (PET) plastic wastes as nanofibrous membranes for oil removal: sustainable solution for plastic waste and oil pollution Ind. Eng. Chem. Res. 61 9077–86
[24] Zhao Z et al 2024 Poly (ethylene terephthalate) micro-nano fibrous membranes via optimized melt electrospinning for water filtration The Journal of The Textile Institute 202407 1–9
[25] Khashij M et al 2022 Recycled PET/metal oxides nanocomposite membrane for treatment of real industrial effluents: Membrane fabrication, stability, antifouling behavior, and process modeling and optimization J. Mol. Liq. 364 119966
[26] Shen K et al 2019 High performance polyamide composite nanofiltration membranes via reverse interfacial polymerization with the synergistic interaction of gelatin interlayer and trimesoyl chloride J. Membr. Sci. 588 117192
[27] Chi X-Y et al 2018 Impact of cross-linked chitosan sublayer structure on the performance of TFC FO PAN nanofiber membranes ACS Omega 3 13009–19
[28] Park M J et al 2018 Hydrophilic polyvinyl alcohol coating on hydrophobic electrospun nanofiber membrane for high performance thin film composite forward osmosis membrane Desalination 426 50–9
[29] Luo F et al 2021 Polydopamine nanoparticles modified nanofiber supported thin film composite membrane with enhanced adhesion strength for forward osmosis J. Membr. Sci. 618 118673
[30] Zhang W-H et al 2024 Stable supra-nanosheet graphene oxide membranes for ultrafast water transport J. Membr. Sci. 711 123160
[31] Park M J et al 2021 Chemically cross-linked graphene oxide as a selective layer on electrospun polyvinyl alcohol nanofiber membrane for nanofiltration application Nanomaterials 11 2867
[32] Khan J and Mariatti M 2021 The influence of substrate functionalization for enhancing the interfacial bonding between graphene oxide and nonwoven polyester Fibers Polym. 22 3192–202
[33] Hut N A et al 2024 Surface decoration of polyethylene terephthalate (PET) waste bottle-derived ultrafiltration membrane for enhanced lead ion removal and antifouling properties J. Environ. Chem. Eng. 12 111766
[34] Jeon E-S et al 2019 A facile and fast transfer of ultrathin graphene oxide film on various substrates J. Phys. D 52 455301
[35] Kumar N et al 2022 Facile scalable synthesis of graphene oxide and reduced graphene oxide: comparative investigation of different reduction methods Carbon Letters 32 1031–46
[36] Selatile K et al 2021 Morphological, thermal, and mechanical properties of electrospun recycled poly (ethylene terephthalate)/graphene oxide composite nanofiber membranes ACS Omega 6 21005–15
[37] Meng L et al 2020 Electrospun nanofiber supports with bio-inspired modification enabled high-performance forward osmosis composite membranes Composites Communications 22 100473
[38] Rashed S H et al 2022 Preparation and characterization of layered-double hydroxides decorated on graphene oxide for dye removal from aqueous solution Journal of Materials Research and Technology 17 2782–95
[39] Gao F et al 2023 Structural properties of graphene oxide prepared from graphite by three different methods and the effect on removal of Cr (VI) from aqueous solution Nanomaterials 13 279
[40] Chen J et al 2020 Molecular insights into the dispersion stability of graphene oxide in mixed solvents: Theoretical simulations and experimental verification J. Colloid Interface Sci. 571 109–17
[41] Tezel T, Ozenc M and Kovan V 2021 Impact properties of 3D-printed engineering polymers Materials Today Communications 26 102161
[42] Wang Z et al 2020 The stability of a graphene oxide (GO) nanofiltration (NF) membrane in an aqueous environment: progress and challenges Materials Advances 1 554–68
[43] Peng C et al 2020 Graphene oxide-based membrane as a protective barrier against toxic vapors and gases ACS Appl. Mater. Interfaces 12 11094–103
[44] Zhao S et al 2020 Graphene-based free-standing bendable films: designs, fabrications, and applications Materials Today Advances 6 100060
[45] Sun J et al 2019 Modulation of cation trans-membrane transport in GO-MoS2 membranes through simultaneous control of interlayer spacing and ion-nanochannel interactions Chemosphere 222 156–64
[46] Kim S et al 2018 Non-swelling graphene oxide-polymer nanocomposite membrane for reverse osmosis desalination J. Membr. Sci. 562 47–55
[47] Mehranbod N et al 2021 Modification and superhydrophilization of electrospun polyvinylidene fluoride membrane using graphene oxide-chitosan nanostructure and performance evaluation in oil/water separation J. Environ. Chem. Eng. 9 106245
[48] Ren J et al 2019 Nanoscale zero-valent iron (nZVI) immobilization onto graphene oxide (GO)-incorporated electrospun polyvinylidene fluoride (PVDF) nanofiber membrane for groundwater remediation via gravity-driven membrane filtration Sci. Total Environ. 688 787–96
[49] Islam M S, Touati K and Rahaman M S 2021 High flux and antifouling thin-film nanocomposite forward osmosis membrane with ingrained silica nanoparticles ACS ES&T Engineering 1 467–77
[50] Karki S et al 2023 Building rapid water transport channels within thin-film nanocomposite membranes based on 2D mesoporous nanosheets Desalination 547 116222